China Steel Technical Report, No. 28, pp.52 −57, (2015)

Numerical Simulation of the Flue Gas Desulfurization in the Sieve Tray Tower

YI-SUNG HUANG*, CHIEN-CHOU TSENG and CHIEN-CHENG CHEN*****

** New Materials Research & Development Department, China Steel Corporation*
*** Department of Mechanical & Electromechanical Engineering, National Sun Yat-sen University*
**** Energy & Resources Department, Technology Division, China Ecotek Corporation*

The coupled effects between the multiphase fluid flows and the corresponding chemical reactions in the wet-type desulfurization tower are modelled in this study. The purpose is to predict the pressure drop and the SO_2 removal efficiency of the sieve tray tower. The real perforated structure cannot be resolved in the computational domain, and hence the validation is carried out first for the pilot plant. From the pilot plant, the results of CFD by real perforated structures and porous media model are very comparable and consistent in the experimental data. Therefore, the porous media model is used to overcome the scale effect of the full-scale desulfurization tower during computation. The results of the numerical simulation for the pressure drop and SO_2 removal efficiency are 141 mmH_2O and 94.3%. Comparatively, the results of the measurement of the sieve tray tower of sinter plant are 126 mmH_2O and 96.0%. Their deviations are 11.9% and 1.8%, respectively. The results show that the numerical simulation can predict the pressure drop and SO_2 removal efficiency accurately as compared with the measurement of the sieve tray tower of sinter plant.

Keywords: **Sieve tray tower, Pilot plant, Porous media model**

1. INTRODUCTION

Sulfur dioxide (SO_2) is usually the major pollutant within the exhaust of the sintering process of the integrated steel plant. China Steel (CSC) has utilized a sieve tray tower to abate SO_2 at the sinter plant as shown in Fig.1(a). The height and diameter of the tower is 23 by 7 m respectively. The exhausted gas from the plant, which mainly contains SO_2, is pumped into the inlet of the desulphurization tower from the pipeline. The inlet Reynolds number Re_{inlet} based on the diameter of the pipeline (3.6 m) is around 2×10^6. As shown in Fig.1(a), there are three sieve trays between the upper and lower nozzles. The lower nozzles simply provide the liquid water to cool down the temperature of the exhausted gas from over 100°C to under 60°C. The upper nozzles inject $Mg(OH)_2$ slurry such that the gaseous SO_2 can be absorbed by the chemical reac-

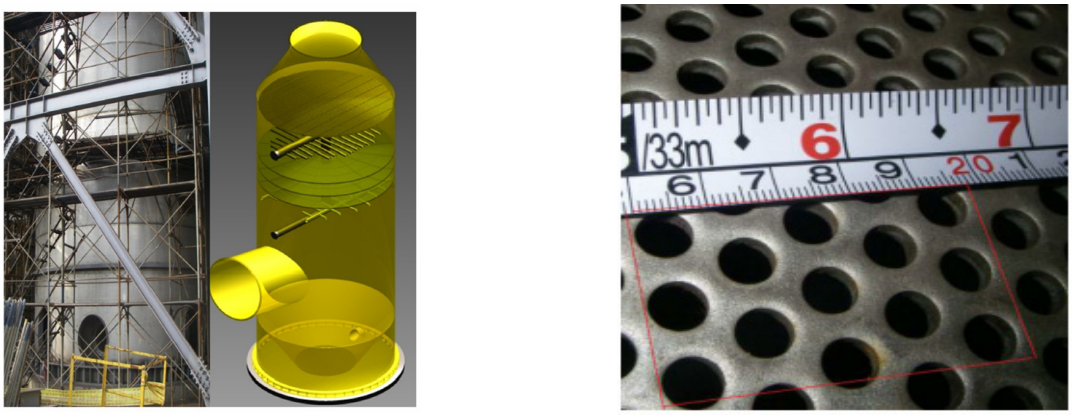

(a) (b)

Fig.1. The schemes show (a) Full-scale desulfurization tower and its detail components by a computer aided program, (b) Perforated structures of the sieve tray.

tions. The slurry then goes to the bottom tank and then is pumped back to the upper nozzles as a closed loop circulation. If the pH of the slurry is too acid, the powders of $Mg(OH)_2$ will be added to the bottom tank to maintain the chemical efficiency. The SO_2 removal efficiency can reach over 95% under the standard operational conditions[1].

The purpose of the three sieve trays between the upper and lower nozzles is to increase the resident time and mixing between the slurry and exhausted gas such that the chemical reaction can be fully utilized. Therefore, the perforated structures of the sieve tray play an important role during the desulfurization process. The representative schematic is shown in Fig.1(b). The perforated holes porosity is 34%, the diameter is 8 mm, the pitch is 13 mm, and the tray thickness is 6 mm. The goal in this study is to simulate the SO_2 removal process and multiphase fluid flowing inside the tower for the optimal efficiency. However, by considering the diameter ratio between the tower (7 m) and the perforated hole diameter (8 mm), the number of perforated holes per sieve tray will exceed 2×10^5, which is computationally too expansive to resolve the sieve tray structures.

As a result, a small scale pilot plant was studied first, a scheme of the pilot plant is illustrated in Fig.2. The nozzles, which spray $Mg(OH)_2$ slurry, are placed above the fourth sieve tray. In the pilot plant, the exhausted gas is cooled down to 58℃ before entering the pilot plant. The Reynolds number based on the diameter of the inlet pipe (0.4 m), Re_{inlet}, is around 1.8×10^5. Although the value is smaller than that of the FGD tower of the sinter plant desulfurization (2×10^6), the dimensionless parameters of perforated structures are very consistent to those of the full scale desulfurization tower in Fig.1(b). For example in the pilot plant, the porosity f is 34.4%, the hole Reynolds number ($Re_h = \rho UD/f\mu$) is 4800, t/D (the ratio of plate thickness to hole diameter) is 0.75, and the value of p/D (the ratio of pitch to hole diameter) is 1.49. The diameter of the tower and perforated holes are 0.6 m and 8 mm, respectively. Due to its smaller scale size, the number of perforated holes per tray is only around 2000. This is manageable for numerical computation even if the detail perforated structure is considered. During the simulation of the pilot plant, the feasibility of the porous media model[2] to replace the real perforated structure of the sieve tray will be evaluated, and this concept will be extended to the full-scale computation as displayed in Fig.1. The objective is to analyze the flow structures and the chemical reaction process within the sieve tray tower such that further optimal design can be carried out.

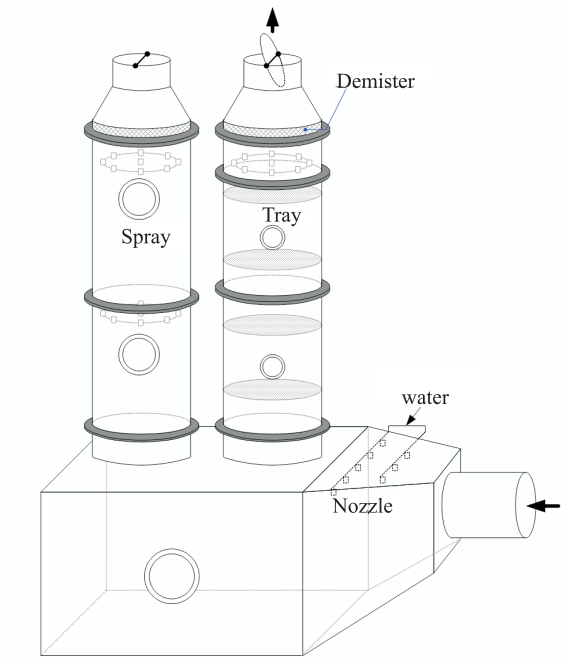

Fig.2. Schematic drawing of the pilot plant.

2. NUMEERICAL METHODS

The current study utilizes the Eulerian-Eulerian method to simulate the multiphase fluid flow interactions between the gas and liquid phases inside the desulfurization tower. Both phases are regards as continuous phases:

$$\frac{\partial}{\partial t}(\alpha_g\rho_g)+\nabla\cdot(\alpha_g\rho_g\vec{v}_g)=0 \quad \text{.....(1)}$$

$$\frac{\partial}{\partial t}(\alpha_l\rho_l)+\nabla\cdot(\alpha_l\rho_l\vec{v}_l)=0 \quad \text{.....(2)}$$

In Equations (1) and (2), α is the volume fraction, ρ is the density, and v is the velocity. The subscript g and l represent those variables for gaseous and liquid phases, respectively. The summations of the liquid volume factions of these two phases are equal to 1. Equations (1) and (2) basically are continuity equation for gaseous and liquid phases, assuming that the mass transfer due to the chemical reaction can be neglected. Similarly, the momentum equations can be listed as below:

$$\frac{\partial}{\partial t}(\alpha_g\rho_g\vec{v}_g)+\nabla\cdot(\alpha_g\rho_g\vec{v}_g\vec{v}_g)=-\alpha_g\nabla p+$$

$$\nabla\cdot\alpha_g(\mu_g+\mu_{g,T})(\nabla\vec{v}_g+\nabla\vec{v}_g^T)+\alpha_g\rho_g\vec{g}+K(\vec{v}_g-\vec{v}_l)$$

.....(3)

$$\frac{\partial}{\partial t}(\alpha_l \rho_l \vec{v}_l) + \nabla \cdot (\alpha_l \rho_l \vec{v}_l \vec{v}_l) =$$

$$-\alpha_l \nabla p + \nabla \cdot \alpha_l (\mu_l + \mu_{l,T})(\nabla \vec{v}_l + \nabla \vec{v}_l^T) + \alpha_l \rho_l \vec{g} + K(\vec{v}_l - \vec{v}_g) \quad \text{..... (4)}$$

Where μ is the dynamic viscosity and the subscript T is the turbulent eddy viscosity, which comes from the RNG k-ε turbulence model[3-5]. K is the empirical-based interchange coefficient that accounts for the interaction force between gaseous and liquid phases.[6] Due to the chemical reaction the momentum transfer can be neglected. The chemical reaction can be described by the species equation:

$$\frac{\partial}{\partial t}(\rho_g \alpha_g Y_{SO_2}) + \nabla \cdot (\rho_g \alpha_g \vec{v}_g Y_{SO_2}) = -S \quad \text{..... (5)}$$

$$\frac{\partial}{\partial t}(\rho_l \alpha_l Y_{Slurry}) + \nabla \cdot (\rho_l \alpha_l \vec{v}_l Y_{Slurry}) = S \quad \text{..... (6)}$$

The gaseous phase includes exhausted air and gaseous SO_2. The mass factions of air and SO_2 inside gaseous phase are denoted as Y_{air} and Yso_2 respectively, and their summation is 1. The gaseous phase density ρ_g in Eqs (1), (3) and (5) then can be expressed as Eq.(7) with ρ_{air} and ρ_{so2} obtained from the equation of states. Similarly for the liquid phase consisting of liquid water and slurry phase.

$$\frac{Y_{SO_2}}{\rho_{SO2}} + \frac{Y_{air}}{\rho_{air}} = \frac{1}{\rho_g} \quad \text{..... (7)}$$

$$\frac{Y_{Slurry}}{\rho_{Slurry}} + \frac{Y_{water}}{\rho_{water}} = \frac{1}{\rho_l} \quad \text{..... (8)}$$

The chemical source term S indicates the transfer rate from gaseous SO_2 into liquid slurry. The chemical reaction includes absorption, dissociation and neutralization. To sum up, the chemical source rate that removes the exhausted SO_2 from the gaseous phase can be expressed as [7]:

$$S = W_{so_2} A_{\text{int}} \left(\frac{1}{k_g^{SO_2}} + \frac{H_{so_2}}{k_l^{SO_2} E_{so_2}}\right)^{-1} (C_g^{SO_2} - H_{so_2} C_l^{SO_2}) \quad \text{.....(9)}$$

The molecular weight of SO_2 is W_{SO_2}, A_{int} is the empirical-based interfacial contact area, the coefficients inside the first bracket are all chemical related constants (Henry constant H, chemical reaction rate k, and enhancement factor E) and the equivalent value of this bracket is 2.95×10^{-5}. $C_g^{SO_2}$ and $C_l^{SO_2}$ represent the mole concentrations of the gaseous phase SO_2 and liquid slurry, respectively. The former is computed from $\rho_g Yso_2/W_{SO_2}$, and while the latter can be tabulated based on Y_{slurry} and pH value[7] from our database.

Computational frameworks from Eqs (1) to (9) consist of the continuity, momentum, and chemical transports. The complex coupling equations from Eqs (1) to (9) are solved by SIMPLC algorithm[8].

3. RESULTS AND DISCUSSION

3.1 The effects of sieve trays in the pilot plant

The pilot plant study of simulation with or without sieve trays to evaluate the effects of sieve trays is illustrated in Fig.3. Figure 3 shows the gaseous flow inside the pilot plant while the nozzles were all turned-off. In other words, only the gaseous phases are considered, and the gaseous volume flow rate from the inlet is 24.07 m^3/min. Figure 3(a) shows the path lines of the gaseous flow when there was no sieve tray inside the tower. It is clear that the gaseous flow tends to occupy the left side of the tower when it makes a 90° turn from inlet to the tower. Therefore, the pathlines inside the tower have more significant components aligned to the horizontal direction. On the other hand, when there were 4 sieve trays placed inside the tower as shown in Fig.3(b), the path lines are almost parallel to the tower.

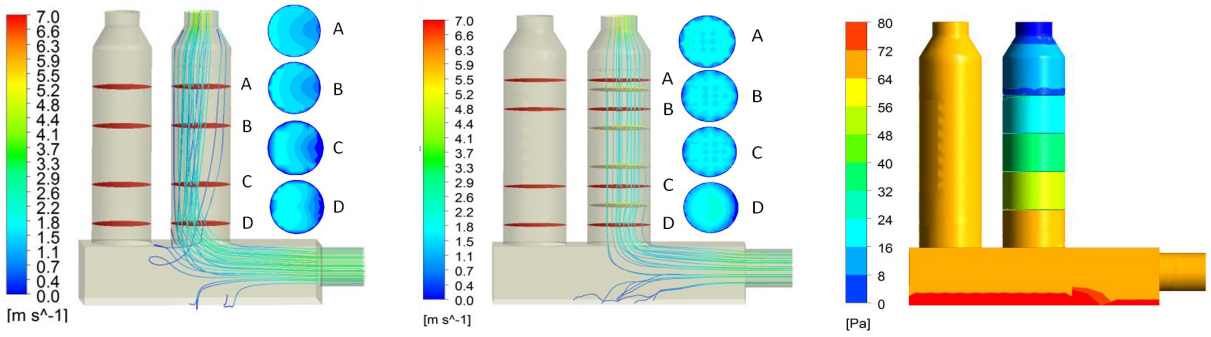

(a) Path lines without trays (b) Path lines with trays (c) Pressure with trays

Fig.3. Scheme of the path lines, velocities and pressure in the pilot plant with 24.07 m^3/min of gas flow rate at inlet.

The small Figures in the right sites of Figs 3(a) and 3(b) show the top views of the velocity distribution of the cross-sections. Due to the implementation of the sieve trays, the velocities become much more uniform and slower in Fig.3(b) than those of Fig.3(a). Figure 3(c) illustrates the pressure contours when the tower is equipped with sieve trays. It is clear the pressure drop only becomes significant across the sieve trays, resulting in a very uniform gaseous velocity distribution inside the tower.

Figure 4 presents similar numerical experiments while only the liquid phases from the nozzles were considered. The liquid volume flow rate from the nozzles was 79.39 l/min. When there were no sieve trays inside the tower as shown in Fig.4(a), the liquid phase velocity was much higher than those shown in Fig.4(b) with sieve trays. Although gravity can accelerate the liquid flow, the sieve trays decelerate it from terminal velocity.

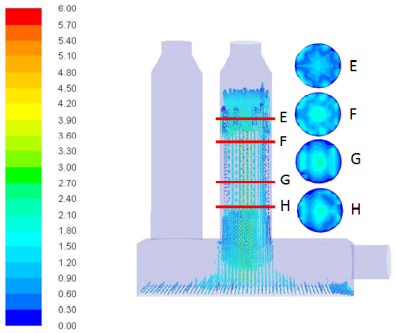

(a) Path lines without trays

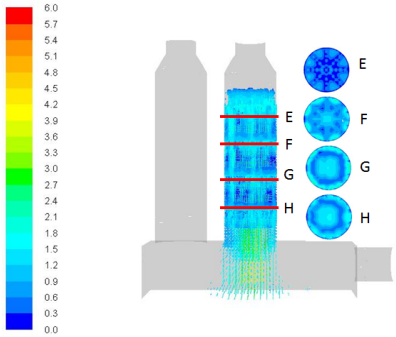

(b) Path lines with trays

Fig.4. Scheme of the path lines and velocities in the pilot plant with 79.39 l/min of liquid flow rate at nozzles.

From the analysis of numerical experiments, the sieve tray can enhance the uniformity of the gaseous phase and decelerate the velocities of both phases. As a result, the mixing between both phases and the residence time inside the tower can be significantly improved by the implementation of sieve trays. Better mixing and longer residence time imply the chemical reaction can be better utilized to remove the gaseous phase SO_2. Figure 5 shows the liquid volume fraction when both phases are considered with and without sieve trays (gaseous flow 24.07 m^3/min; liquid flow 79.39 l/min). When the tower was empty, the left-tendency of the gaseous flow shown in Fig.3(a) squeezes the liquid flow from the nozzles to the right side of the tower in Fig.5(a). On the other hand, the liquid phase accumulated above the sieve trays as shown in Fig.5(b), which illustrates evidence of better mixing between the liquid and gas phases when the sieve trays were implemented.

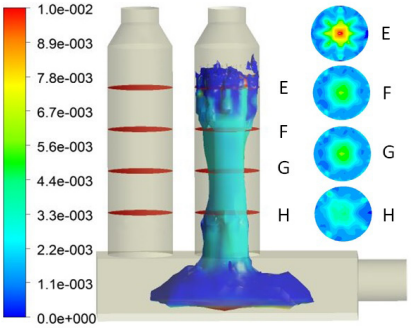

(a) Without trays

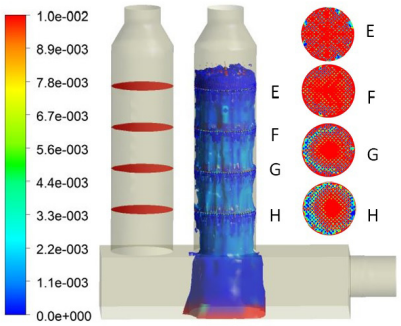

(b) With trays

Fig.5. The liquid volume fraction when both phases are considered.

Figure 6 shows the mass fraction of the gaseous SO_2 in terms of different L/G ratio (liquid to gas volume flow rate) while the gaseous volume flow rate was kept as 24 m^3/min, and the mass fraction of the gaseous phase SO_2 from inlet was 4.63×10^{-4} (200 ppm). From L/G= 2-6, the mass fraction of SO_2 as L/G= 6 was much less than that of L/G= 2 because stronger chemical reactions occurred when more liquid slurry was injected from nozzles. The numerical results are compared with the experimental measurements at different monitor locations, namely G_{t3} and G_{t4} shown in Fig.6. Table 1 shows that the numerical and experimental results of SO_2 removal efficiency are largely consistent, which validates our current numerical framework.

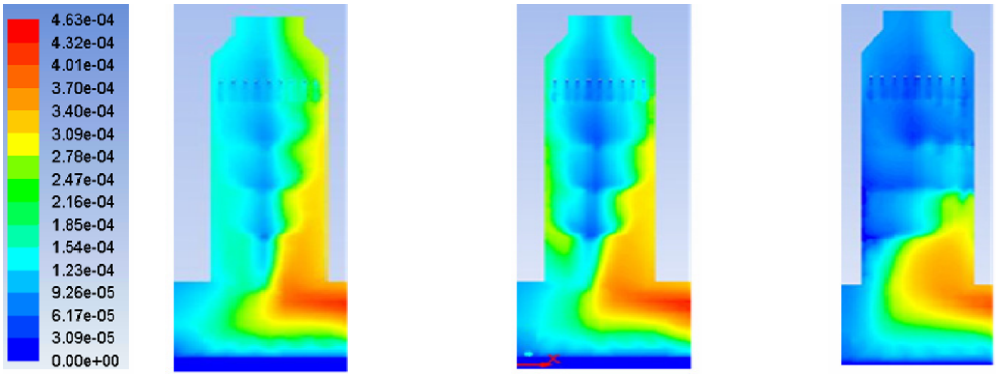

(a) L/G= 2 (b)L/G= 4 (c) L/G= 6

Fig.6. The mass fraction of gaseous SO_2 at different L/G.

Table 1 The SO_2 removal efficiency at different sampling locations for the pilot plant

	L/G=2		L/G=4		L/G=6	
	G_{t3}	G_{t4}	G_{t3}	G_{t4}	G_{t3}	G_{t4}
Experimental results	54.0%	66.0%	49.0%	68.0%	59.0%	78.0%
Real perforated structure	47.3%	59.0%	56.4%	66.5%	69.0%	76.4%
Porous media model	48.5%	56.0%	54.0%	64.6%	69.7%	76.7%

3.2 The gaseous SO_2 distribution inside the pilot plant and porous media model

The number of perforated holes for each sieve tray inside the pilot plant is approximately 2000, however, this value becomes 2×10^5 when almost the same structures of the sieve tray are applied to the full-scale tower Fig.1. Therefore, the porous media model is considered here. The idea is to skip the detail in grid layouts to capture the perforated structures in the computational domain by simply using a momentum source term in Eq.(10) into the momentum Eqs (3) and (4).

$$B_i = -(C_2 \frac{1}{2}\rho|u|u_i)/t \quad \text{..... (10)}$$

In Equation (10), t is the tray thickness and C_2 is the inertial loss coefficient. C_2 is tunable and can be estimated from empirical equation[9] or computed from unit method approach[10]. Based on the current porosity f (34.4%), the hole Reynolds number (4800), t/D (0.75) and the p/D (1.51), C_2 can be tabulated as 9.83 empirically for both phases within the sieve tray[9]. Table 1 also compares the numerical results by the real perforated structures and porous media model. It is clearly these two numerical results that are very comparable while results by the porous media model can significantly reduce the number of the grid points. After the validation of the pilot plant, this porous media model and C_2 value can be further applied to the full scale computation of Fig.1 in the next section.

3.3 The details inside the full-scale tower

Because the detail of the perforated structure is beyond the computation power for the full-scale tower, the porous media model is implemented into the governing equations based on the previous section. The SO_2 concentration from the inlet pipeline is 200 ppm, and the gaseous volume flow rate is 12000 m^3/min. The liquid volume flow rate from the nozzles is 1200 m^3/min. Figure 7(a) shows that a significant pressure drop is only observed across the sieve tray, and the SO_2 distribution inside the tower is illustrated in Fig.7(b).

The validations between measurement and numerical results are listed in Table 2. The pressure drop and SO_2 removal efficiency are based on the corresponding

Table 2 The validation between measurement and computational results

	CFD	Measurement	Deviation (%)
SO_2 removal efficiency (%)	94.3	96.0	1.8
Pressure drop (mmH_2O)	141.0	126.0	11.9

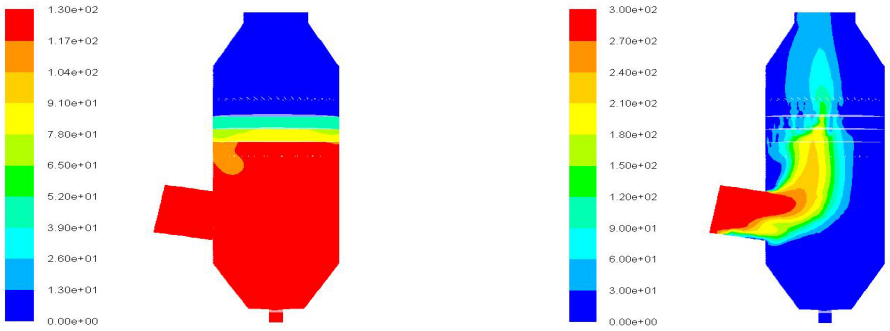

(a) Pressure drop (mmH_2O) (b) SO_2 concentration (ppm)

Fig.7. The pressure drop and SO_2 distribution inside the full-scale tower.

values between the inlet and outlet of the tower. And Table 2 shows that the current numerical framework can even match the full-scale situation, hence it can be utilized further as an optimal design tool.

4. CONCLUSIONS

The couple effects between the multiphase fluid flow and the corresponding chemical reactions are modelled in this study. The purpose is to predict the pressure drop and the SO_2 removal efficiency of the desulfurization tower. Due to the scale effect, the real perforated structure cannot be resolved in the computational domain, and hence the validation is carried out first for the small scale pilot plant.

For the pilot plant, the effects of the sieve tray are studied. It shows that the sieve trays can enhance the uniformity of the fluid flow and slow down the velocity. Therefore, better mixing and longer residence time can be obtained to improve the chemical reaction. Furthermore, from the small scale pilot plant, the CFD results by real perforated structures and porous media model are very comparable and consistent to the experimental data. Therefore, the porous media model is used to overcome the scale effect of the full-scale desulfurization tower during computation.

The results of the numerical simulation for the pressure drop and SO_2 removal efficiency are 141 mmH_2O and 94.3%. Comparatively, the results of the measurement of the sieve tray tower of sinter plant are 126 mmH_2O and 96.0%. The deviations of both of them are 11.9% and 1.8%, respectively. The results show that the numerical simulation can predict the pressure drop and SO_2 removal efficiency very well as compared with the measurement of the sieve tray tower of sinter plant. Consequently, further optimal design for the sieve tray tower can be conducted by the computation to gain first-hand information.

REFERENCES

1. Kubota Kasui Corporation, 2015. http://www.fkk.co.jp/wp/pdf/k_airtech.pdf
2. A. Szymkiewicz, "Mathematical Models of Flow in Porous Media", Modelling Water Flow in Unsaturated Porous Media, Springer Berlin Heidelberg, vol. 9, no. 47, 2013.
3. W. P. Jones and B. E. Launder, "The Prediction of Laminarization with a Two-equation Model of Turbulence", International Journal of Heat and Mass Transfer, vol. 15, no. 2, pp. 301-304, 1972.
4. B. E. Launder and D. B. Spalding, The Numerical Computation of Turbulent Flows, Computer Methods in Applied Mechanics and Engineering, vol. 3, no. 2, pp. 269-289, 1974.
5. W. Shyy, S. S. Thakur, H. Ouyang, J. Liu and E. Blosch, Computational Techniques for Complex Transport Phenomena, Cambridge University Press, 2005.
6. Lijun Ji et al., "Momentum Exchange Coefficient for Two Jet Flows Mixing in a Tee Junction", Frontiers of Chemical Engineering in China, pp. 1-5, 2009.
7. L. Marocco and F. Inzoli, "Multiphase Euler Lagrange CFD Simulation Applied to Wet Flue Gas Desulfurization Technology", International Journal of Multiphase Flow, vol. 35, no. 2, pp. 185-194, 2009.
8. J. P. Van Doormaal and G. D. Raithby, "Enhancements of the Simple Method for Predicting Incompressible Fluid Flows", Numerical Heat Transfer, vo. l7, no. 2, pp. 147-163, 1984.
9. P. L. Smith and M. Van Winkle, Discharge Coefficients Through Perforated plates at Reynolds Numbers of 400 to 3000, AIChE Journal, vol. 4, no. 3, pp. 266-268, 1958.
10. B.Y. Guo, Q. F. Hou, A. B. Yu, L. F. Li and J. Guo, Numerical Modelling of the Gas Flow Through Perforated Plates, Chemical Engineering Research and Design, vol. 91, no. 3, pp. 403-408, 2013. □